INTERNATIONAL JOURNAL FOR NUMERICAL METHODS IN ENGINEERING
Int. J. Numer. Meth. Engng 2001; **50**:2521–2545

Dispersion analysis of stabilized finite element methods for acoustic fluid interaction with Reissner–Mindlin plates

Lonny L. Thompson*,† and Sridhar Sankar

Department of Mechanical Engineering, Clemson University, Clemson, SC 29634, U.S.A.

SUMMARY

The application of stabilized finite element methods to model the vibration of elastic plates coupled with an acoustic fluid medium is considered. A complex-wavenumber dispersion analysis of acoustic fluid interaction with Reissner–Mindlin plates is performed to quantify the accuracy of stabilized finite element methods for fluid-loaded plates. Results demonstrate the improved accuracy of a recently developed hybrid least-squares (HLS) plate element based on a modified Hellinger–Reissner functional, consistently combined with residual-based methods for the acoustic fluid, compared to standard Galerkin and Galerkin gradient least-squares plate elements. The technique of complex wavenumber dispersion analysis is used to examine the accuracy of the discretized system in the representation of free waves for fluid-loaded plates. The influence of fluid and coupling matrices resulting from consistent implementation of pressure loading in the residual for the plate equation is examined and clarified for the different finite element approximations. Copyright © 2001 John Wiley & Sons, Ltd.

KEY WORDS: finite element methods; Reissner–Mindlin plates; fluid–structure interaction; structural acoustics

1. INTRODUCTION

When modelling the steady-state response of structures coupled with an acoustic fluid, plate and shell elements are needed to accurately represent both subsonic, leaky, and evanescent wave types in the solution. Subsonic waves are characterized by propagating waves in the plate with a real-valued wavenumber with modulus larger than the sonic wavenumber of the acoustic fluid. Leaky waves are characterized by complex wavenumber roots where the real part is much larger than the imaginary part. For high frequencies, the energy associated with leaky waves will propagate with decay within the plate, while slowly 'leaking' energy into the

*Correspondence to: Lonny L. Thompson, Department of Mechanical Engineering, Clemson University, 102 Floor Daniel Engineering Innovation Building, Box 340921, Clemson, SC 29634-0921, U.S.A.
†E-mail: lonny.thompson@ces.clemson.edu

Contract/grant sponsor: NSF PECASE; contract/grant number: CMS-9702082

Received 16 May 2000
Revised 2 August 2000

Copyright © 2001 John Wiley & Sons, Ltd.

fluid. Evanescent wavenumbers occur as complex conjugate pairs over the entire frequency range. This root represents a solution that decays rapidly in the plate and is important near discontinuities such as stiffeners or point loads. The accurate resolution of these wave types is especially important when modelling sound wave interaction in applications of structural acoustics. Standard four-node quadrilateral displacement-based plate and shell elements such as the mixed interpolation with shear projection (MITC4), and selectively reduced integration elements (SRI4) [1], while eliminating shear locking problems for thin plates, exhibit poor accuracy at high frequencies. To solve this problem, new stabilized hybrid plate elements have been developed based on a generalized least-squares modification to the underlying Hellinger–Reissner functional [2, 3]. The least-squares operators are proportional to residuals of the governing equations of motion for Reissner-Mindlin plates in stress-resultant form. The inclusion of shear deformation and rotary inertia effects in this theory is important for high-frequency response for flexural waves in plates. Use of independent displacements and stress resultants in this hybrid least-squares (HLS) method provides a general framework for enhancing the accuracy of mixed/hybrid plate elements. In References [2, 3], complex-wavenumber finite element dispersion analysis is used as a design criteria to select optimal tuning parameters in the HLS formulation so that for a given wave propagation angle, the plate elements match the analytical wavenumber–frequency relations for *in vacuo* plates exactly. In this paper, our strategy is to combine these HLS plate elements with stabilized treatments for the acoustic fluid for accurate response of fluid-loaded Reissner–Mindlin plates. The residual-based Galerkin least-squares (GLS) methods developed in Reference [4], and the stabilized methods (STB) developed in Reference [5], are considered. Both fluid stabilization treatments are residual-based methods which improve the accuracy of the finite element approximation to the sonic wavenumber.

Complex-wavenumber dispersion analysis is used to examine the accuracy of free waves in the HLS plate elements developed in References [2, 3], coupled with stabilized methods for the fluid [4, 5]. We use complex-wavenumber dispersion analysis as a tool for quantifying the behaviour of different combinations of stabilized methods for acoustic–structure interaction. While based on the study of infinite plates, dispersion analysis provides a valuable tool for predicting the general trends in behaviour for finite element discretization of practical models with fixed boundaries. The use of finite element dispersion analysis for fluid-loaded plate systems was first performed by Jasti [6], where real-valued free waves in Galerkin-based plate elements using both Kirchoff's theory and Mindlin's theory, coupled with a Galerkin formulation for the fluid were studied. Later, Grosh and Pinsky [7] extended his work to include imaginary wavenumbers, and helped to clarify the significance of each wavenumber branch.

Weighted residuals of the governing Euler–Lagrange equations in least-squares form were first used to stabilize the pathologies exhibited by the classical Galerkin method for the numerical solution of advection–diffusion problems [8]. These so-called Galerkin least-squares (GLS) stabilized methods have been successfully employed in a wide variety of applications where enhanced stability and accuracy properties are needed. These ideas have since been extended in Reference [9], and Reference [4] for the GLS finite element solution to the scalar Helmholtz equation governing wave propagation in acoustic fluids. In References [4, 10], finite element dispersion analysis was used to select optimal mesh parameters in the least-squares modifications to the standard Galerkin method, resulting in improved phase accuracy for both two- and three-dimensional acoustic problems.

Copyright © 2001 John Wiley & Sons, Ltd.

The first use of residual-based methods for static analysis of plate structures can be found in Reference [11], where symmetric forms of the equilibrium equations were appended to the standard Galerkin equations to improve accuracy. Later, Grosh and Pinsky [12] applied the Galerkin gradient least-squares (GGLS) method of Franca [13] to improve the accuracy of Timoshenko beam elements for steady-state vibration. In Reference [14], the GGLS Timoshenko beam element is combined with the one-dimensional GLS method of Harari [9] to study acoustic-fluid loaded beams. As expected, the combined use of stabilized methods for both the beam and acoustic fluid, yielded improved accuracy over standard Galerkin methods. However, as mentioned in Reference [12], the extension of the GGLS formulation to Reissner–Mindlin plate elements based on bi-linear displacement interpolation failed to produce a general four-node quadrilateral element which is free from shear locking, limiting the use of this method for practical applications. Our approach for modelling fluid-loaded structures is similar to that used in Reference [14]. Here, instead of a Galerkin-based displacement method, we use the locking free, quadrilateral plate elements based on the hybrid least-squares (HLS) method developed in References [2, 3], combined with the improved acoustic fluid stabilization methods developed in References [4, 5]. Using a consistent combination of accurate HLS methods for the uncoupled plate and GLS methods for the fluid, improved methods are obtained such that the finite element dispersion relations closely match each branch of the complex wavenumber loci for fluid-loaded plates.

In the following, we first summarize the analytical dispersion relation for *in vacuo* Reissner–Mindlin plates. This dispersion relation is used to design hybrid least-squares (HLS) plate elements which for a given free-wave angle, exactly match the analytical wavenumber–frequency relation for *in vacuo* plates. Next, the analytical subsonic, leaky, and evanescent roots for the fluid-loaded plate are derived, and then compared to the coupled finite element formulation with different stabilized fluid treatments. The accuracy of different finite element approximations for the fluid-loaded plate system are examined and clarified using complex-wavenumber dispersion analysis. Finally, conclusions are made and future work is discussed.

2. REISSNER–MINDLIN PLATE EQUATIONS

Consider a plate of thickness t, defined on the domain Ω_s such that,

$$\Omega_s = \left\{ (x, y, z) \in R^3,\ z \in \left[-\frac{t}{2}, \frac{t}{2} \right], (x, y) \in \Gamma \subset R^2 \right\} \tag{1}$$

where Γ is a two-dimensional midsurface and z is the co-ordinate transverse to this plane. Furthermore, loading $q(x, y)$ is restricted to the direction normal to the midsurface defined as $\mathbf{e}_z$.

Mindlin's approximate theory for flexural waves in plates includes shear deformation and rotary inertia effects which are important for high-frequency excitation. The deformation at any point is given by the three-dimensional displacement vector defined by the kinematic relation, $\mathbf{u} = -z\boldsymbol{\theta}(x, y) + w(x, y)\mathbf{e}_z$, where $\boldsymbol{\theta} = [\theta_x, \theta_y]^{\mathrm{T}}$ denotes the two-dimensional vector of rotations, such that $\boldsymbol{\theta} \perp \mathbf{e}_z$. The components θ_x and θ_y are the rotations of the transverse line elements (perpendicular fibres to the midsurface) about the y- and x-axis, respectively. As a consequence of the kinematic assumptions, the in-plane bending strains $(\varepsilon_{xx}, \varepsilon_{yy}, \gamma_{xy})$,

Copyright © 2001 John Wiley & Sons, Ltd.

are linearly related to curvatures through a differential operator $\mathbf{L}$, acting on the rotations $\boldsymbol{\theta}$,

$$\boldsymbol{\kappa} = \mathbf{L}\,\boldsymbol{\theta} = [\theta_{x,x}\,,\ \theta_{y,y}\,,\ \theta_{x,y} + \theta_{y,x}]^{\mathrm{T}} \tag{2}$$

Using first-order shear deformation theory, the transverse shear strains are defined by the angle between the slope of the midsurface after deformation and the fibre orientation,

$$\boldsymbol{\gamma} = \nabla w - \boldsymbol{\theta} = [w_{,x} - \theta_x\,,\ w_{,y} - \theta_y]^{\mathrm{T}} \tag{3}$$

For classical Kirchoff thin plate theory, the slope is assumed to be equal to the fibre rotation so that $\boldsymbol{\gamma} = 0$. The inclusion of non-zero shear deformation in the Reissner–Mindlin model allows for a more accurate representation of high-frequency behaviour.

For a homogeneous plate with linear elastic material properties, the constitutive relation for the bending and twisting moments $\mathbf{M} = [M_x\,,\ M_y\,,\ M_{xy}]^{\mathrm{T}}$ and shear resultants $\mathbf{Q} = [Q_x\,,\ Q_y]^{\mathrm{T}}$ is given by, $\mathbf{M} = \mathbf{D}_{\mathrm{b}}\,\boldsymbol{\kappa}$, and $\mathbf{Q} = D_{\mathrm{s}}\,\boldsymbol{\gamma}$, where for isotropy,

$$\mathbf{D}_{\mathrm{b}} = D_{\mathrm{b}} \begin{bmatrix} 1 & \nu & 0 \\ \nu & 1 & 0 \\ 0 & 0 & \dfrac{(1-\nu)}{2} \end{bmatrix}, \quad D_{\mathrm{b}} = \frac{EI}{(1-\nu^2)}, \quad D_{\mathrm{s}} = G_{\mathrm{s}} t \tag{4}$$

with $I = t^3/12$, Young's modulus E, Poisson's ratio ν, shear modulus G, and κ is a shear correction factor, $G_{\mathrm{s}} = \kappa G$.

For time-harmonic motion, the coupled equations of motion for the *in vacuo* Reissner–Mindlin plate may be expressed in terms of generalized displacements $\mathbf{u}^* = [w, \theta_x, \theta_y]$, and stress resultants $\boldsymbol{\sigma}^* = [\mathbf{M}, \mathbf{Q}]$. Here we write the equilibrium equations as residuals, R_1, and $\mathbf{R}_2 = [R_{2x}, R_{2y}]^{\mathrm{T}}$,

$$R_1[\mathbf{u}^*, \boldsymbol{\sigma}^*] := \nabla \cdot \mathbf{Q} + m\,\omega^2\,w + q = 0 \tag{5}$$

$$\mathbf{R}_2[\mathbf{u}^*, \boldsymbol{\sigma}^*] := \mathbf{L}^{\mathrm{T}}\,\mathbf{M} + \mathbf{Q} + \rho I\,\omega^2\,\boldsymbol{\theta} = \mathbf{0} \tag{6}$$

In the above, $m = \rho t$ is the mass density per unit area, ω is the circular frequency measured in rad/s, and $\mathbf{L}$ is the differential operator implied in (2).

In the absence of an applied load q, the plate equations of motion admit solutions of the form

$$w = w_0 \mathrm{e}^{(\mathrm{i}k\boldsymbol{\nu}\cdot\mathbf{x})}, \quad \boldsymbol{\theta} = \theta_0 \boldsymbol{\nu} \mathrm{e}^{(\mathrm{i}k\boldsymbol{\nu}\cdot\mathbf{x})} \tag{7}$$

In the above, $\mathrm{i} = \sqrt{-1}$, k is the wavenumber, $\boldsymbol{\nu} = [\cos\varphi\,,\ \sin\varphi]$ defines a unit vector in the direction of wave propagation, with wave vector $\mathbf{k} = k\boldsymbol{\nu} = k[\cos\varphi\,,\ \sin\varphi]$. Conditions for the allowed waves are obtained by substituting the assumed exponentials (7) for $\mathbf{u}^*$ into the homogeneous equations of motion. Two independent characteristic equations associated with transverse deflection and rotation result:

$$\begin{bmatrix} D_{\mathrm{s}}k^2 - \rho t\,\omega^2 & \mathrm{i}k\,D_{\mathrm{s}} \\ -\mathrm{i}k\,D_{\mathrm{s}} & D_{\mathrm{b}}k^2 + D_{\mathrm{s}} - \rho I\omega^2 \end{bmatrix} \begin{Bmatrix} w_0 \\ \theta_0 \end{Bmatrix} = \begin{Bmatrix} 0 \\ 0 \end{Bmatrix} \tag{8}$$

Copyright © 2001 John Wiley & Sons, Ltd.

Non-trivial solutions for the wave amplitudes w_0 and θ_0 are obtained by setting the determinant of the characteristic matrix to zero. The result is the dispersion equation relating frequency ω to wavenumber k,

$$\mathscr{D}(k) := \left(k^4 - \lambda_s^2 k^2 - \lambda_b^4\right) = 0 \tag{9}$$

with frequency-dependent functions,

$$\lambda_s^2 = \left[k_s^2 + k_p^2\right], \quad \lambda_b^4 = \left[k_b^4 - k_p^2 k_s^2\right] \tag{10}$$

Here, $k_p = \omega/c_p$, $k_s = \omega/c_s$, $k_b = (m\omega^2/D_b)^{1/4}$, where k_b is the classical plate bending wavenumber for *in vacuo* flexural waves in the Kirchoff theory, and

$$c_p = \left[\frac{E}{\rho(1-\nu)^2}\right]^{1/2}, \quad c_s = \left(\frac{G_s}{\rho}\right)^{1/2}$$

Considered as a function of k^2, solutions to the plate dispersion relation (9) occur in pairs: $\pm k_1$ and $\pm k_2$. At frequencies below a cut-off frequency, the wavenumber pair $\pm k_1$ occurs as purely real, while the pair $\pm k_2$ is purely imaginary. The real wavenumber pair corresponds to propagating waves while the imaginary pair corresponds to evanescent waves characterized by exponential decay. The influence of the evanescent waves are localized near drivers and discontinuities in the plate, e.g. near boundary layers. In the next section, the discrete counterpart to this continuous dispersion relation is used as a tool for the design of stabilized hybrid finite element methods, which for a given free-wave angle, match the exact wavenumber-dispersion relation defined by (9).

3. HYBRID LEAST-SQUARES FORMULATION

In References [2, 3] a new hybrid least-squares (HLS) finite element method based on a modified Hellinger–Reissner functional with independent stress and displacement approximations was developed. The Hellinger–Reissner functional is modified by adding weighted differential operators acting on the residuals of the governing equations of motion for the plate written in least-squares form. This approach may be considered an extension of Galerkin least-squares (GLS) methods to mixed/hybrid methods. For the Mindlin plate equations, the HLS functional is expressed in terms of the residuals R_1, and $\mathbf{R}_2 = [R_{2x}, R_{2y}]$, as [3],

$$F_{\mathrm{HLS}}(\mathbf{u}^*, \boldsymbol{\sigma}^*) = F_{\mathrm{H}}(\mathbf{u}^*, \boldsymbol{\sigma}^*) + \frac{1}{2}\int_{\tilde{\Gamma}} \tau_1 (\nabla R_1)^2 \, \mathrm{d}\Gamma + \frac{1}{2}\int_{\tilde{\Gamma}} \tau_2 \{(R_{2x,x})^2 + (R_{2y,y})^2\} \, \mathrm{d}\Gamma \tag{11}$$

In the above, $\tilde{\Gamma} = \cup_e \Gamma_e$ is the union of element interiors Γ_e, and $F_{\mathrm{H}}(\mathbf{u}^*, \boldsymbol{\sigma}^*)$ defines the Hellinger–Reissner functional for the plate equations of motion,

$$F_{\mathrm{H}}(\mathbf{u}^*, \boldsymbol{\sigma}^*) = F_b + F_s - \omega^2 \frac{1}{2}\int_{\Gamma} (mw^2 + \rho I \boldsymbol{\theta}^2) \, \mathrm{d}\Gamma \tag{12}$$

Copyright © 2001 John Wiley & Sons, Ltd.

with

$$F_{\mathrm{b}}(\boldsymbol{\theta}, \mathbf{M}) := \int_{\Gamma} \mathbf{M}^{\mathrm{T}} \boldsymbol{\kappa} \, \mathrm{d}\Gamma - \frac{1}{2} \int_{\Gamma} \mathbf{M}^{\mathrm{T}} \mathbf{D}_{\mathrm{b}}^{-1} \mathbf{M} \, \mathrm{d}\Gamma \tag{13}$$

$$F_{\mathrm{s}}(\mathbf{u}^{*}, \mathbf{Q}) := \int_{\Gamma} \mathbf{Q}^{\mathrm{T}} \boldsymbol{\gamma} \, \mathrm{d}\Gamma - \frac{1}{2} \int_{\Gamma} \mathbf{Q}^{\mathrm{T}} D_{\mathrm{s}}^{-1} \mathbf{Q} \, \mathrm{d}\Gamma \tag{14}$$

The frequency-dependent parameters $\tau_1 = \tau_1(\omega)$ and $\tau_2 = \tau_2(\omega)$ are local mesh parameters determined from dispersion analysis and designed to stabilize the finite element solution, thus improving accuracy [2, 3]. Setting $\tau_1 = \tau_2 = 0$, reverts to the underlying hybrid formulation. The use of residuals maintains the consistency of the resulting finite element variational equation. Integration of the residuals over element interiors $\tilde{\Gamma}$ is required to maintain C^0 continuity between adjacent elements.

Using a mixed/hybrid finite element approach, *independent* approximations are used for the displacement variables and stress resultants—a compatible displacement field $\mathbf{u}^{*} = \mathbf{N}\mathbf{d}$, and a local stress field defined within element interiors $\boldsymbol{\sigma}^{*} = \mathbf{P}\boldsymbol{\beta}$. Here, $\mathbf{N}$ and $\mathbf{P}$ are arrays of polynomial basis functions and $\mathbf{d}$ and $\boldsymbol{\beta}$ are the unknown element nodal degrees of freedom (dof) and stress parameters, respectively. Any of several existing mixed finite element approximation fields which produce elements which are free from shear locking and pass the static patch test may be used. In References [2, 3], we used the field-consistent displacement and assumed stress fields proposed by Aminpour [15] to develop a four-node hybrid least-squares quadrilateral plate element (HLS4). The transverse displacement interpolation is bi-linear in the nodal parameters w_i, enriched with linked quadratic functions expressed in terms of the nodal rotations θ_{xi} and θ_{yi}. The transverse displacement is approximated by polynomials of one order higher than the rotations resulting in a field consistent basis. The curvatures and shear strains are then formed by, $\boldsymbol{\kappa} = \mathbf{B}_{\mathrm{b}}\mathbf{d}$, and $\boldsymbol{\gamma} = \mathbf{B}_{\mathrm{s}}\mathbf{d}$, defined by (2) and (3), respectively. The assumed moment $\mathbf{M} = \mathbf{P}_{\mathrm{b}}\boldsymbol{\beta}$, and shear force $\mathbf{Q} = \mathbf{P}_{\mathrm{s}}\boldsymbol{\beta}$, fields are formulated in element natural co-ordinates and then transformed into physical co-ordinates by means of the contravariant tensor transformation evaluated at the centre of the element. The shear resultant field satisfies *a priori* the static equilibrium equations defined in natural co-ordinates. To simplify the residuals in the least-squares modification for distorted elements, we neglect the effect of scaled mixed derivatives and assume the shear resultants satisfy the static conditions $\mathbf{Q} = -\mathbf{L}^{\mathrm{T}}\mathbf{M}$, and $\nabla \cdot \mathbf{Q} = 0$ within an element.

Imposing stationary conditions with respect to $\mathbf{u}^{*}$ and $\boldsymbol{\sigma}^{*}$, and eliminating $\boldsymbol{\beta}$ from the resulting discrete Euler–Lagrange equations results in the dynamic stiffness matrix for each element:

$$\mathbf{s}^{e}(\omega) = \mathbf{k}^{e} - \omega^{2}\,\mathbf{m}^{e} + \mathbf{k}_{\mathrm{LS}}^{e}(\omega) \tag{15}$$

The element stiffness matrix is constructed from

$$\mathbf{k}^{e} = \mathbf{T}^{\mathrm{T}}\mathbf{H}^{-1}\mathbf{T} \tag{16}$$

where

$$\mathbf{T} = \int_{\Gamma_e} \mathbf{P}_{\mathrm{b}}^{\mathrm{T}}\mathbf{B}_{\mathrm{b}} \, \mathrm{d}\Gamma + \int_{\Gamma_e} \mathbf{P}_{\mathrm{s}}^{\mathrm{T}}\mathbf{B}_{\mathrm{s}} \, \mathrm{d}\Gamma \tag{17}$$

$$\mathbf{H} = \int_{\Gamma_e} \mathbf{P}_{\mathrm{b}}^{\mathrm{T}}\mathbf{D}_{\mathrm{b}}^{-1}\mathbf{P}_{\mathrm{b}} \, \mathrm{d}\Gamma + \int_{\Gamma_e} \mathbf{P}_{\mathrm{s}}^{\mathrm{T}} D_{\mathrm{s}}^{-1}\mathbf{P}_{\mathrm{s}} \, \mathrm{d}\Gamma \tag{18}$$

The consistent element mass $\mathbf{m}^{e}$ is computed in standard form.

Copyright © 2001 John Wiley & Sons, Ltd.

For general four-node quadrilateral finite elements with the stress fields defined by Aminpour [15], we determine the frequency-dependent stabilization matrix $\mathbf{k}^e_{\mathrm{LS}}$ from the simplified form

$$\mathbf{k}^e_{\mathrm{LS}}(\omega) = r_1(\omega)\mathbf{k}^e_{\mathrm{LS1}} + r_2(\omega)\mathbf{k}^e_{\mathrm{LS2}} \tag{19}$$

with frequency-independent matrices,

$$\mathbf{k}^e_{\mathrm{LS1}} = \int_{\Gamma_e} \{\mathbf{N}^{\mathrm{T}}_{w,x}\mathbf{N}_{w,x} + \mathbf{N}^{\mathrm{T}}_{w,y}\mathbf{N}_{w,y}\}\,\mathrm{d}\Gamma \tag{20}$$

$$\mathbf{k}^e_{\mathrm{LS2}} = \int_{\Gamma_e} \{\mathbf{N}^{\mathrm{T}}_{\theta_x,x}\mathbf{N}_{\theta_x,x} + \mathbf{N}^{\mathrm{T}}_{\theta_y,y}\mathbf{N}_{\theta_y,y}\}\,\mathrm{d}\Gamma \tag{21}$$

where $\mathbf{N}_w(\xi,\eta)$, $\mathbf{N}_{\theta_x}(\xi,\eta)$ and $\mathbf{N}_{\theta_y}(\xi,\eta)$ are row vectors of polynomial basis functions defined by finite element approximations in natural co-ordinates (ξ,η): $w = \mathbf{N}_w\mathbf{d}^e$, $\theta_x = \mathbf{N}_{\theta_x}\mathbf{d}^e$, $\theta_y = \mathbf{N}_{\theta_x}\mathbf{d}^e$. In the above, $r_1 = \tau_1(m\omega^2)^2$ and $r_2 = \tau_2(\rho I\omega)^2$ are scaled mesh parameters. Here, we have assumed r_i, $i = 1,2$ are constant within an element Γ_e, although variable r_i are possible. In References [2, 3], optimal values for r_1 and r_2 are determined such that finite element wavenumber pairs $\pm k_1$ and $\pm k_2$ match the analytical wavenumber pairs for a given wave orientation angle φ on a uniform mesh. In the asymptotic limit $\omega \to 0$, we require the frequency-dependent design parameters to satisfy the property $r_1 \to 0$, and $r_2 \to 0$. This restriction maintains the static properties of the underlying hybrid plate element, i.e. no shear locking or spurious modes. We note that this requirement in the zero-frequency limit was not enforced in the GGLS method used in Reference [12] for 1-D Timoshenko beams, thus limiting direct extension to 2-D arbitrary quadrilateral plates.

Figure 1 shows a comparison of finite element and analytical dispersion curves for the propagating and evanescent wave numbers for a steel plate *in vacuo*. Results are given for a uniform mesh with waves directed along mesh lines. The dispersion curves are compared for the mixed interpolation of tensorial components element (MITC4) [1], the hybrid element (HYB4) of [15], and the hybrid-least-squares element (HLS4), [2, 3]. For propagation along mesh lines, results for MITC4 are equivalent to SRI4. The properties for the plate are taken as: $E = 210 \times 10^{10}$ dynes/cm^2, $\nu = 0.29$, $\rho = 7.8$ g/cm^2, and $\kappa = 5/6$. The ratio of the element length-to-plate thickness is $h/t = 1.0$. For reference, the frequency is normalized with respect to the element length h, and the speed of sound in water, $c_0 = 148\,100$ cm/s. The MITC element significantly under-estimates the propagating real wavenumber pair while overestimating the imaginary wavenumber. The HYB element matches the analytical propagating wavenumber much better, suggesting significant improvement in phase accuracy. The HLS element matches the analytical dispersion curves *exactly* by design.

4. COUPLED ACOUSTIC FLUID-PLATE EQUATIONS

For the fluid loaded plate, the acoustic pressure $p(x,y,z)$ appears as a surface traction in the vertical equation of motion for the plate:

$$Q_{x,x} + Q_{y,y} + m\omega^2 w(x,y) = p(x,y,0) - q(x,y), \quad (x,y) \in \Gamma \tag{22}$$

Copyright © 2001 John Wiley & Sons, Ltd.

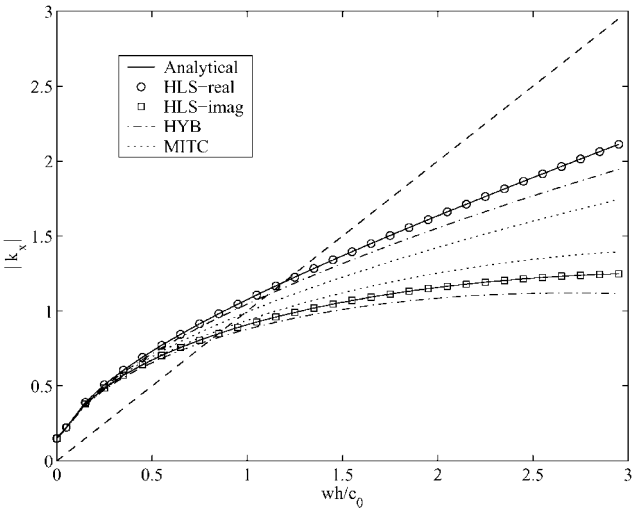

Figure 1. Comparison of analytic and finite element dispersion curves for steel plate *in vacuo* with $h/t = 1.0$. k_1 (propagating) and k_2 (evanescent) wavenumber pairs for hybrid least-squares (HLS), hybrid (HYB), and (MITC). The sonic wavenumber $k_0 = \omega/c_0$, denoted by dashed lines, is shown for reference.

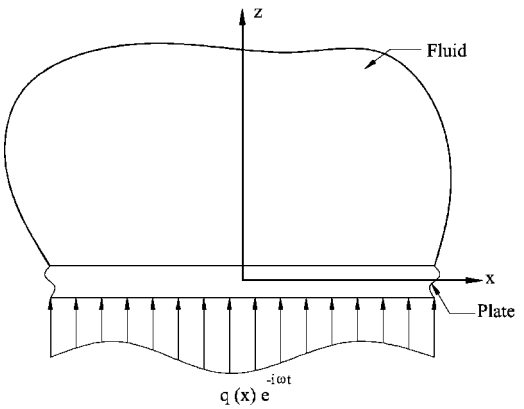

Figure 2. Schematic of fluid-loaded plate.

The fluid domain Ω_f is defined by the semi-infinite region $z \geqslant 0$, see Figure 2. The bottom of the plate is assumed to be *in vacuo*. The acoustic pressure satisfies the Helmholtz equation

$$(\nabla^2 + k_0^2)\, p(x, y, z) = 0, \quad (x, y, z) \in \Omega_f \tag{23}$$

where $k_0 = \omega/c_0$, and $c_0 = K/\rho_0$ is the acoustic wave speed. To ensure outgoing waves, the acoustic pressure is also subject to the Sommerfeld radiation condition at infinity. The continuity of normal acceleration on the wet surface $z = 0$, is expressed as the Neumann condition

$$\left.\frac{\partial p}{\partial z}\right|_{z=0} = \rho_0 \omega^2 w(x, y) \quad \text{on } \Gamma \tag{24}$$

Copyright © 2001 John Wiley & Sons, Ltd.

Here we assume free plane waves propagating in the x-direction within the fluid-loaded plate with no sources $q = 0$. The plate vertical deflection w and rotation $\theta = \theta_x$ is sought in the following form:

$$w = w_0 e^{ik_x x}, \quad \theta = \theta_0 e^{ik_x x} \tag{25}$$

With these conditions, the functions w, θ, and p are independent of y, so that the governing plate equations can be simplified to

$$Q_{x,x} + m\omega^2 w(x) = p(x,z)|_{z=0} \tag{26}$$

$$M_{x,x} + Q_x + \rho I \omega^2 \theta(x) = 0 \tag{27}$$

Eliminating θ in favour of w gives the single equation:

$$w_{,xxxx} + \lambda_s^2 w_{,xx} - \lambda_b^4 w = \frac{1}{D_s}[\lambda_p^2 p + p_{,xx}]|_{z=0} \tag{28}$$

with frequency-dependent functions λ_b, λ_s, defined in (10), and

$$\lambda_p^2 = \left[k_p^2 - D_s/D_b\right]$$

Assuming a plane wave solution for acoustic pressure:

$$p(x,z) = p_0 e^{i(k_x x + k_z z)} \tag{29}$$

then to satisfy (23) and (24),

$$p(x,z) = \frac{\rho_0 \omega^2}{ik_z} w_0 e^{i(k_x x + k_z z)} \tag{30}$$

with k_z defined by

$$k_0^2 = k_x^2 + k_z^2 \tag{31}$$

The dispersion equation for the fluid-loaded plate is obtained by introducing (25) and (30) into the plate equation (28), with the result

$$ik_z D_s \mathscr{D}(k_x) - \rho_0 \omega^2 \left(\lambda_p^2 - k_x^2\right) = 0 \tag{32}$$

In the above $\mathscr{D}(k_x)$ is the dispersion equation for *in vacuo* plates defined in (9). The roots of this equation give the possible wavenumbers k_x and k_z of the free plane waves. Squaring both sides of (32) and using (31) to eliminate k_z in terms of k_x, the dispersion equation for fluid-loaded plates can be replaced by

$$D_s^2 (k_0^2 - k_x^2)(k_x^4 - \lambda_s^2 k_x^2 - \lambda_b^4)^2 - \rho_0^2 \omega^4 (\lambda_p^2 - k_x^2)^2 = 0 \tag{33}$$

Considered as an equation in k_x^2, the dispersion equation has five roots; One subsonic wavenumber (purely real), two Leaky wavenumbers, and two evanescent wavenumbers (occur as complex conjugate pairs). Once the k_x^2 roots have been computed, the components k_z are obtained from (31).

Copyright © 2001 John Wiley & Sons, Ltd.

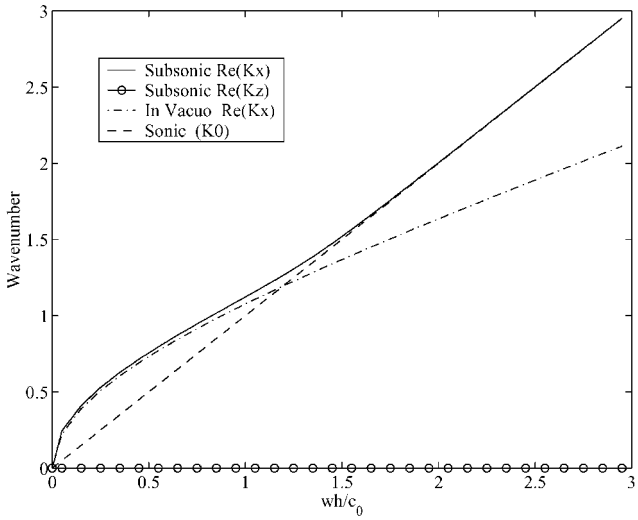

Figure 3. Fluid-loaded plate analytical dispersion relation for the subsonic root. The propagating root for the in vacuo plate k_1, and sonic wavenumber $k_0 = \omega h/c_0$, are plotted for reference. The *coincident frequency* $\omega h/c_0 = 1.13$, for the fluid-loaded plate is located at the intersection where the $k_1 = k_0$.

There is one real k_x root over all frequencies with modulus larger than the acoustic wavenumber k_0. Since $k_x > k_0$, this root is interpreted as a *subsonic* free wave. The subsonic root is plotted in Figure 3 using the fluid-loaded plate properties given earlier, and with fluid density $\rho_0 = 1.0$ g/cm^3. The *coincident frequency* $\omega h/c_0 = 1.13$, for the fluid-loaded plate is located at the intersection where the *in vacuo* propagating wavenumber for the plate, k_1, matches the sonic wavenumber $k_0 = \omega/c_0$. Below coincidence, the subsonic wave behaves as a modified propagating wave in the plate. For frequencies above coincidence, the subsonic wavenumber asymptotes to the sonic line $k_0 = \omega h/c_0$. For this root, $k_z^2 = k_0^2 - k_x^2 < 0$, so that the component $k_z = \mathrm{i}(k_x^2 - k_0^2)^{1/2}$ is purely imaginary, and the acoustic pressure decreases exponentially with respect to the variable z. The energy associated with this wave is trapped in the acoustic near field of the plate, and decays rapidly in the fluid.

The two leaky wavenumbers are characterized by the roots where the real part of k_x is much larger than the imaginary part, i.e. $\mathrm{Re}(k_x) \ll \mathrm{Im}(k_x)$, see Figure 4. In the region $k_0 < k_1$, the k_x component of the leaky wavenumbers initially occur as complex conjugate pairs and then quickly bifurcate into two paths of pure real roots such that $k_0 < k_x < k_1$. As the frequency increases, the paths rejoint to form a complex conjugate pair. For frequencies beyond the intersection of the real part of the leaky root k_x, and the sonic root k_0, then $\mathrm{Re}(k_x) < k_0$. For these higher frequencies, the energy associated with the leaky wave will propagate with decay within the plate, while slowly 'leaking' energy into the fluid with wave angle defined by $\alpha = \arctan \mathrm{Re}(k_z/k_x)$.

The two evanescent wavenumbers occur as complex conjugate pairs over the entire frequency range, with $\mathrm{Im}(k_x) \gg \mathrm{Re}(k_x)$, see Figure 5. This root represents a solution that decays rapidly in the plate. For the steel plate in water, the evanescent wavenumber closely matches the imaginary root of the *in vacuo* plate over all frequencies, i.e., $\mathrm{Im}(k_x) \sim k_2$. The energy

Copyright © 2001 John Wiley & Sons, Ltd.

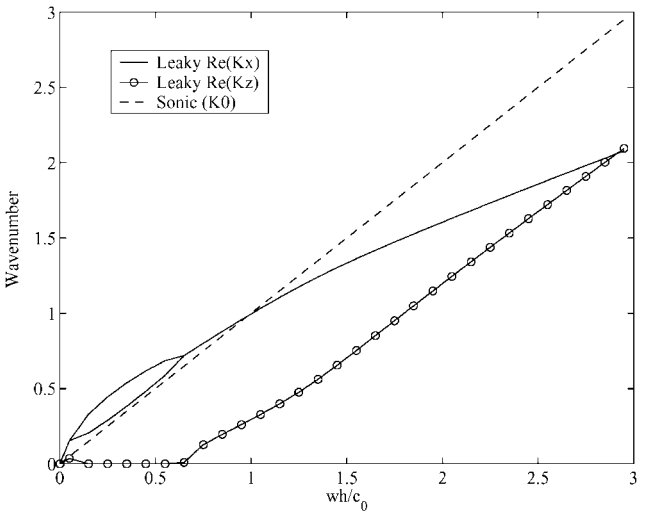

Figure 4. Fluid-loaded plate analytical dispersion relation for the real part of the two leaky roots.

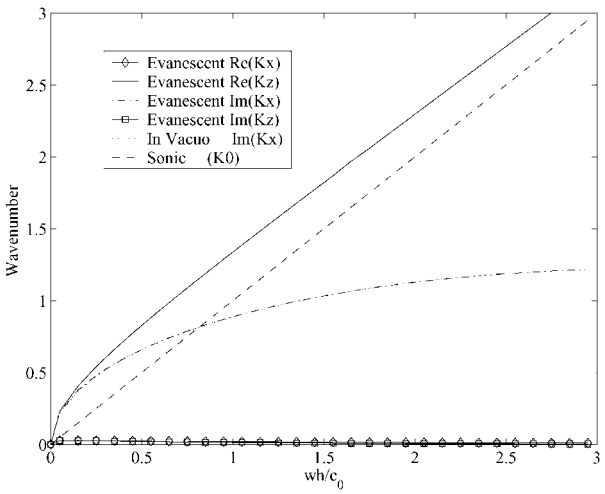

Figure 5. Fluid-loaded plate analytical dispersion relation for the complex conjugate evanescent roots. The imaginary root for the *in vacuo* plate k_2, and sonic wavenumber K_0, are plotted for reference.

associated with the evanescent wave is radiated nearly perpendicular to the plate with a propagating wavenumber $\mathrm{Re}(k_z)$ which asympotes to a line tangent to the sonic wavenumber k_0.

While not all of the roots can be considered free waves over all frequencies, the location of each root plays a role in asymptotic and numerical evaluations of analytical solutions for fluid-loaded plates [16, 17]. Below coincidence, the leaky roots to the dispersion relation (33) generally have the least influence on analytical solutions, compared to subsonic and evanescent roots [16]. From these observations, while all roots of the fluid-loaded dispersion relation

Copyright © 2001 John Wiley & Sons, Ltd.

have significance, we conjecture that the subsonic and evanescent waves should be most closely matched by any finite element approximation, with the subsonic the most important for accurate phase in structures with widely spaced discontinuities.

4.1. Stabilized finite element formulation

Our stabilized variational formulation for the coupled fluid–structure problem may be stated in terms of the variation of a functional,

$$\delta(F_{\mathrm{s}} + F_{\mathrm{f}}) = \delta W \tag{34}$$

where the structural part $F_{\mathrm{s}} = F_{\mathrm{HLS}}(\mathbf{u}^*, \boldsymbol{\sigma}^*, p)$ is the hybrid-least-squares functional defined earlier for the plate, with the residual R_1, modified for the fluid pressure loading p on the plate, i.e.

$$R_1 = \nabla \cdot \mathbf{Q} + m\,\omega^2\, w + q - p|_{z=0} \tag{35}$$

The fluid part $F_{\mathrm{f}} = F_{\mathrm{GLS}}(p)$ is defined by a Galerkin functional modified by a residual in least-squares form over element interiors and a residual over inter-element boundaries:

$$F_{\mathrm{GLS}}(p) = F_{\mathrm{G}}(p) + \frac{1}{2}\int_{\tilde{\Omega}_{\mathrm{f}}} \tau\,(\nabla^2 p + k_0^2\, p)^2\,\mathrm{d}\Omega + \int_{\mathscr{S}'} \beta\,[\![\, p_{,n} \,]\!](\nabla^2 p + k_0^2\, p)\,\mathrm{d}\mathscr{S} \tag{36}$$

$$F_{\mathrm{G}}(p) = \frac{1}{2}\int_{\Omega_{\mathrm{f}}} (\nabla p)^2\,\mathrm{d}\Omega + \frac{1}{2}k_0^2 \int_{\Omega_{\mathrm{f}}} p^2\,\mathrm{d}\Omega \tag{37}$$

In the above, $\mathscr{S}' = \cup_e\, \mathscr{S}_e$ is the union of inter-element boundaries $\mathscr{S}_e$, $[\![\, p_{,n} \,]\!]$, denotes a jump in normal derivatives across element boundaries, τ and β are mesh parameters designed to stabilize the uncoupled acoustic fluid problem. For $\tau = 0, \beta = 0$ the formulation reverts to Galerkin. The term involving the element parameter τ is in the form of a standard Galerkin least-squares operator [9, 4]. The form for the residual of normal derivatives across element boundaries associated with the parameter β is motivated by the residual-based method given in Reference [5].

The right-hand side is the 'virtual work' of the interface conditions, coupling the structure to the fluid,

$$\delta W = \int_{\Gamma} \delta w\,(q - p)\,\mathrm{d}\Gamma - \rho_0 \omega^2 \int_{\Gamma} \delta p\, w\,\mathrm{d}\Gamma \tag{38}$$

Introducing finite element approximations for the acoustic pressure $p = \mathbf{N}_p\,\mathbf{p}$, together with the displacement and stress approximations for the plate discussed earlier, and imposing stationary conditions with respect to p, and $(\mathbf{u}^*, \boldsymbol{\sigma}^*)$, leads to the symmetric coupled system of equations for the stabilized fluid-loaded plate elements,

$$\begin{bmatrix} \mathbf{s}^e & \mathbf{q}^e \\ \mathbf{q}^{e\mathrm{T}} & \mathbf{h}^e \end{bmatrix} \begin{Bmatrix} \mathbf{d}^e \\ \mathbf{p}^e \end{Bmatrix} = \begin{Bmatrix} \mathbf{f}^e \\ 0 \end{Bmatrix} \tag{39}$$

Copyright © 2001 John Wiley & Sons, Ltd.

where $\mathbf{s}^e$ is the structure dynamic stiffness matrix defined in (15), and $\mathbf{h}^e = \mathbf{h}_{\mathrm{f}} + \mathbf{h}_{\mathrm{LS}}$, and $\mathbf{q}^e = \mathbf{c} + \mathbf{c}_{\mathrm{LS}}$, are the fluid dynamic stiffness and structure–fluid coupling matrices, respectively. Here, $\mathbf{h}_{\mathrm{f}} = (\mathbf{k}_{\mathrm{f}} - k_0^2\mathbf{m}_{\mathrm{f}} + \mathbf{k}_{\mathrm{LS}}^{\mathrm{f}})/(\rho_0\omega^2)$, is the fluid dynamic stiffness matrix composed of standard fluid stiffness $\mathbf{k}_{\mathrm{f}}$, and mass matrices $\mathbf{m}_{\mathrm{f}}$, resulting from discretization of the Helmholtz equation, and a frequency-dependent, residual-based stabilization matrix, $\mathbf{k}_{\mathrm{LS}}^{\mathrm{f}}(\omega)$, associated with the mesh parameters τ and β, as described in References [4, 5]. For shear fields in the hybrid element satisfying static equilibrium, i.e. $\nabla \cdot \mathbf{Q} = 0$, the contribution to the fluid matrix resulting from the pressure loading appearing in the structural residual R_1, is defined by $\mathbf{h}_{\mathrm{LS}} = [h_{\mathrm{LS}}^{ij}]$

$$h_{\mathrm{LS}}^{ij} = \frac{r_1}{(m\omega^2)^2} \int_{\tilde{\Gamma}} \nabla N_p^i \cdot \nabla N_p^j \, \mathrm{d}\Gamma \tag{40}$$

The matrix $\mathbf{c}^e$ defines the coupling matrix resulting from (38), while $\mathbf{c}_{\mathrm{LS}}$ defines the stabilization matrix resulting from the coupling of w, and the pressure loading p, in the variational term associated with the residual R_1, i.e.

$$-\frac{r_1}{m\omega^2} \left(\int_{\tilde{\Gamma}} \nabla \delta w \cdot \nabla p \, \mathrm{d}\Gamma + \int_{\tilde{\Gamma}} \nabla \delta p \cdot \nabla w \, \mathrm{d}\Gamma \right) \tag{41}$$

For waves restricted to the xz-plane it is sufficient to consider a one-dimensional simplification of the plate model with $\nabla = \partial/\partial x$, coupled to a fluid mesh defined by two-dimensional four-node bilinear acoustic elements. In this case, the residuals simplify and we consider two alternatives for τ and β in the fluid functional defined in (36). In the first, we consider only the residual within an element and set $\beta = 0$. In this case, the GLS parameter $\tau(k_0 h)$ is defined by [4]

$$\tau k_0^2 = 1 - \frac{6(4 - f_x - f_z - 2f_x f_z)}{(k_0 h)^2 (2 + f_x)(2 + f_z)} \tag{42}$$

where $f_x = \cos(k_0 h \cos \pi/8)$, $f_z = \cos(k_0 h \sin \pi/8)$, $k_0 = \omega/c_0$, and h represents the element size.

In the second case, we consider both the least-squares residual within element interiors associated with τ, and residuals defined on inter-element boundaries associated with β. Here, the values which produce a leading order $O((k_0 h)^7)$ correction to the finite element approximation to the sonic wavenumber k_0^h, are defined by [5]

$$8\tau k_0^2 = \tau_1 + \tau_2(\xi^2 + \eta^2) - 90\xi^2\eta^2 \tag{43}$$

$$8\beta k_0^2 = -20 + 15(\xi^2 + \eta^2) \tag{44}$$

where the coefficients $\tau_1(k_0 h)$ and $\tau_2(k_0 h)$ have the following dependence on $k_0 h$:

$$\begin{aligned} \tau_1 &= -10 - \tfrac{13}{6}(k_0 h)^2 - \tfrac{9}{640}(k_0 h)^4 \\ \tau_2 &= 30 + \tfrac{9}{4}(k_0 h)^2 - \tfrac{67}{768}(k_0 h)^4 \end{aligned} \tag{45}$$

In the above, ξ, η, denote natural co-ordinates defined on a bi-unit reference element. Natural co-ordinates are used to parameterize general quadrilateral elements in physical co-ordinates.

Copyright © 2001 John Wiley & Sons, Ltd.

In general, the small amount of extra computation required by including residuals on element boundaries with the parameters defined above is worth the effort for acoustic problems, since the sonic wavenumber accuracy is improved compared to the first case with $\beta = 0$. However as discussed in the next section, when combined with the interaction with plate discretization, the accuracy is not necessarily superior for the fluid-loaded plate problem.

The dispersion analysis and numerical example for the residual-based method applied to fluid-loaded beams given in the main body of Reference [14] used an unsymmetric variational equation resulting from a weighting (test) function which neglects the pressure loading term in the residual for R_1. This method is properly defined as a Petrov–Galerkin method (*not* least-squares), and leads to an unsymmetric system matrix with increased memory requirements. The inclusion of the pressure loading in the residual of the shear equations of motion in (35) provides a consistent and naturally symmetric variational formulation for the fluid-loaded plate model, similar to that given in Reference [14, Appendix A]. Here, instead of a Galerkin-based displacement method, we use the locking free hybrid least-squares (HLS) plate elements based on the modified Hellinger–Reissner functional, consistently combined with the improved acoustic fluid stabilization methods developed in References [4, 5]. Recently, in Reference [18], the symmetric GGLS method given in Appendix A of Reference [14] has been shown to give improved accuracy over the Galerkin and Petrov–Galerkin methods for the fluid-loaded beam numerical example used in [14, Section 5.2]. No dispersion analysis of the symmetric GGLS method was performed.

5. FINITE ELEMENT DISPERSION ANALYSIS

Finite element dispersion relations for the fluid-loaded plate are obtained by assembling a patch of elements from a uniform mesh with grid spacing $\Delta x = \Delta z = h$ [6, 7]. The result is three repetitive stencils associated with solutions $\mathbf{v}_n = [w_n, \theta_n, p_{n,0}, p_{n,1}]^{\mathrm{T}}$, at a typical node n:

$$\sum_{l=-1}^{1} \mathbf{B}_l \mathbf{v}_{n+l} = 0 \tag{46}$$

Here $\mathbf{B}_l$ are (3×4) matrix partitions which depend on frequency and the element dynamic stiffness coefficients. The notation $p_{n,0}$ denotes pressure solutions at a node lying on the plate boundary at $z = 0$, while $p_{n,1}$ denotes solutions at a typical node along the first row of grid points in the fluid defined by $z = h$.

The dispersion relation for the uncoupled fluid relating wavenumber components k_x and k_z, to frequency $k_0 = \omega/c_0$ is given by [4, 21]

$$g_2 c_z + g_1 = 0 \tag{47}$$

$$g_2 = (c_x h_{13} + h_{14}), \quad g_1 = (c_x h_{12} + h_{11}) \tag{48}$$

with $c_z = \cos(k_z h)$, $c_x = \cos(k_x h)$, $s_x = \sin(k_x h)$, and $h_{ij} = [\mathbf{h}^e]_{ij}$, are frequency-dependent coefficients of the fluid dynamic stiffness matrix.

Copyright © 2001 John Wiley & Sons, Ltd.

To obtain finite element dispersion relations for the coupled fluid–plate system, free waves are assumed at a typical node along the x-direction of the plate,

$$\begin{Bmatrix} w_n \\ \theta_n \end{Bmatrix} = \begin{Bmatrix} w_0 \\ \theta_0 \end{Bmatrix} \mathrm{e}^{(\mathrm{i}k_x\, n\, h)} \tag{49}$$

Similarly, pressure solutions at a typical node are assumed in exponential form in the xz-plane,

$$p_{n,m} = p_0 \mathrm{e}^{(\mathrm{i}k_x nh)}\, \mathrm{e}^{(\mathrm{i}k_z nh)} \tag{50}$$

The dispersion relations for the fluid-loaded plate are obtained by substituting (49) and (50) into stencils (46) and using (47) to eliminate k_z. The result are the coupled wavenumber–frequency relations defined by the Hermitian matrix

$$\begin{bmatrix} S_{11} & -\mathrm{i}S_{12} & Q_1 \\ \mathrm{i}S_{12} & S_{22} & -\mathrm{i}Q_2 \\ Q_1 & \mathrm{i}Q_2 & H_1 \end{bmatrix} \begin{Bmatrix} w_0 \\ \theta_0 \\ p_0 \end{Bmatrix} = \begin{Bmatrix} 0 \\ 0 \\ 0 \end{Bmatrix} \tag{51}$$

The above coefficients are functions of k_x and ω. The functions associated with the structural difference equations are, $S_{11} = s_{13}\, c_x + s_{11}$, $S_{22} = s_{24}\, c_x + s_{22}$, $S_{12} = s_{23}\, s_x$. For the coupling equations, $Q_1 = q_{12}\, c_x + q_{11}$, $Q_2 = q_{41}\, c_x$; Fluid equations, $H_1 = \pm (g_1^2 - g_2^2)^{1/2}$. Here $s_{ij} = [\mathbf{s}^e]_{ij}$, and $q_{ij} = [\mathbf{q}^e]_{ij}$, are coefficients of the element dynamic stiffness arrays for the 1-D plate model coupled to four-node acoustic elements; further details are given in References [6, 7, 19, 20]. The fluid-loaded plate dispersion equation relating wavenumber k_x to frequency ω is obtained by rooting the characteristic polynomial obtained from the determinant of (51). Six root pairs k_x are computed—five of which closely approximate the analytical roots determined from (33). Once the k_x roots have been computed, the components k_z are obtained from (47). While the finite element dispersion relation is written in terms of dynamic stiffness coefficients of 1-D plate elements coupled with four-node acoustic elements, it can be shown that this same relation between k_x and ω holds for a uniform mesh of 2-D plate elements coupled to 3-D acoustic 'brick' elements with waves associated with k_x propagating along mesh lines.

Figure 6 shows the dispersion error in the subsonic and real part of the leaky root using the MITC plate element combined with a Galerkin fluid approximation. Results are reported as the relative phase error for wavenumber k_x with element length to plate thickness $h/t = 1$. Figure 7 (top) shows the relative phase error in the finite element approximation to the subsonic wavenumber k_x^h, for the stabilized methods. The subsonic wavenumber often plays a dominant role in fluid-loaded plates. Thus by reducing the percent error in the subsonic wavenumber, even if by a small amount, the overall accuracy of the numerical solution can increase significantly. Results for the MITC4 plate element with a Galerkin approximation for the fluid (MITC-Gal) gives very large errors, both below and above the coincident frequency. With this discretization, the error is greater than 6 per cent at coincidence. In contrast, the hybrid plate element with Galerkin least-squares approximation for the fluid (HYB-GLS) reduces the error significantly to less than 2 per cent at coincidence. The hybrid least-squares plate element together with GLS for the fluid (HLS-GLS) improves the accuracy even further, closely matching the analytical wavenumber, with less than 1 per cent error at coincidence. The Galerkin gradient-least-squares (GGLS) plate element developed in Reference [12] is also compared. Here we use the symmetric coupling of Reference [14, Appendix A], with GLS fluid

Copyright © 2001 John Wiley & Sons, Ltd.

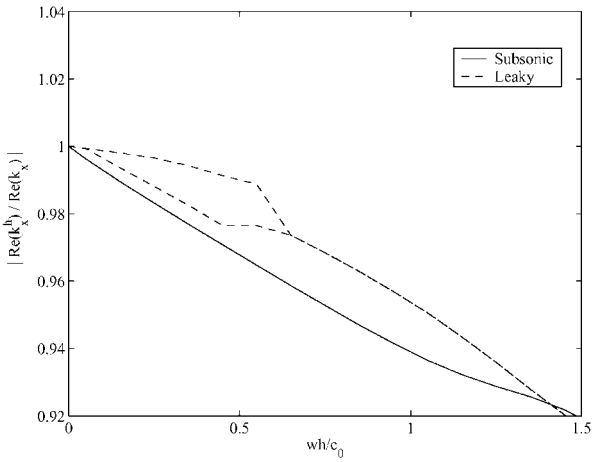

Figure 6. Dispersion error for MITC plate element combined with Galerkin fluid approximation. Relative error for real part of subsonic and leaky roots k_x with $h/t = 1$.

elements with the improved mesh parameter τ given in (42). We note that this GGLS plate element is restricted to rectangular elements only. Below coincidence $\omega h/c_0 = 1.13$, GGLS-GLS shows significant error and then approaches the HYB-GLS solution for frequencies higher than coincidence. When the GLS fluid representation is replaced with the stabilized term defined by the τ and β parameters defined in (43), and (44), which includes residuals on the boundary, the phase accuracy is decreased below coincidence. However, above coincidence, where the fluid properties dominate the behaviour of the root, the stabilized fluid approximation (STB), with a better approximation to the sonic wavenumber, quickly improves the dispersion error. Below coincidence, the GLS fluid phase error partially cancels the plate discretization error leading to a lower overall dispersion error for the HLS-GLS structure–fluid combination.

Figure 7 (bottom) shows the relative dispersion error in the real part of the leaky wavenumber k_x for the stabilized methods. The sharp peak occurs near the end of the bifurcation region at $\omega h/c_0 = 0.6$, where the leaky roots change from separate real roots, to a complex-conjugate pair. The spike in the error is a result of missing the bifurcation point by a small amount. As mentioned earlier, we conjecture that since this error peak occurs before coincidence, where the leaky wavenumbers have relatively small influence on the overall solution, the impact on the finite element solution is small compared to accuracy of the subsonic or evanescent roots. In the bifurcation region, the HYB-GLS solution matches the analytical wavenumber closely. However, after rejoining to form a pair of complex-conjugate roots, HYB-GLS underestimates the analytical wavenumbers. The HLS-GLS solution closely matches the analytical leaky component over the entire frequency range. Accuracy of the leaky roots decreases for the STB fluid compared to GLS. Similar to the subsonic wavenumber results, the leaky wavenumber solutions for GGLS-GLS show significant error prior to coincidence. The solution using MITC4 with Galerkin fluid completely misrepresents the leaky wavenumbers both in the bifurcation and complex-conjugate regions (not shown).

Copyright © 2001 John Wiley & Sons, Ltd.

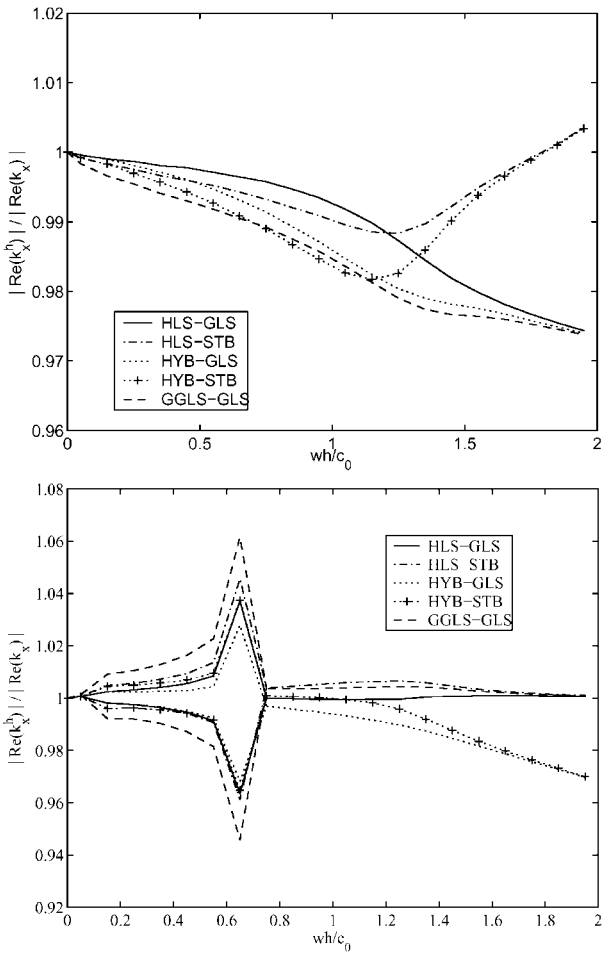

Figure 7. Relative error in real part of wavenumber k_x for stabilized methods. (top) subsonic, (bottom) leaky.

Figure 8 shows the amplitude error in the imaginary part of the leaky and evanescent roots using the MITC plate element combined with a Galerkin fluid approximation. Figure 9 (top) shows the relative error for $\mathrm{Im}(k_x)$, measured as an error in amplitude decay for the stabilized methods. Results show significant error in the evanescent wavenumber using the MITC-Gal combination. With this discretization, the amplitude error at coincidence is 6 per cent. The Hybrid plate element with GLS or STB fluid stabilization reduces the error to 1 per cent at coincidence. Of notice is both HLS-GLS, HLS-STB and GGLS-GLS evanescent wavenumbers match the analytical value over the entire range of frequencies. The similarities in the evanescent wavenumbers is explained by the dominant influence of the common treatment for the *in vacuo* plate evanescent wavenumber k_2, where both HLS and GGLS are designed to exactly match k_2 along mesh lines and over all frequencies. Since the evanescent wavenumber

Copyright © 2001 John Wiley & Sons, Ltd.

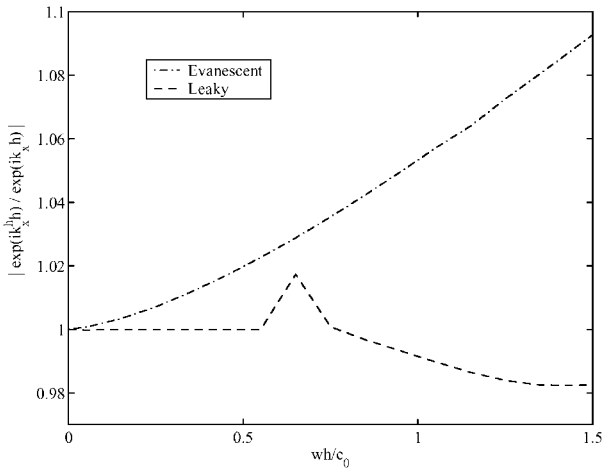

Figure 8. Amplitude error for MITC plate element combined with Galerkin fluid approximation. Relative error for imaginary part of leaky and evanescent roots k_x with $h/t = 1$.

$\mathrm{Im}(k_x) \sim k_2$, the amplitude error for the fluid-loaded plate is small using HLS. Figure 9 (bottom) shows the amplitude error for the imaginary part of the leaky wavenumber $\mathrm{Im}(k_x)$ for the stabilized methods. Here both HLS-GLS and HYB-GLS give errors less than 1 per cent. The error is largest for the GGLS-GLS method.

The relative error in $\mathrm{Re}(k_y)$ for the stabilized methods, is shown in Figure 10. Dispersion error in the fluid due to evanescent roots is similar for the plate elements with common GLS fluid treatment, increasing steadily with increasing frequency. In contrast, the STB treatment for the fluid shows very small error. This result demonstrates the strong influence of the improved sonic wavenumber accuracy on the dispersion error. The phase error for propagating waves in the fluid due to the leaky roots is the smallest using HLS-GLS. Again, the large peak occurs due to the small misrepresentation of the bifurcation point corresponding to frequency $\omega h/c_0 = 0.6$.

Comparison of amplitude error due to imaginary components $\mathrm{Im}(k_z)$ are shown in Figure 11. Before coincidence, the STB fluid treatment shows improved accuracy for the amplitude of the evanescent root compared to GLS. For the amplitude of the leaky root, above coincidence, the STB method for fluid tends to underestimate the exact value. In contrast, the GLS method overestimates the exact value. HLS-GLS gives the best overall accuracy for this wavenumber component.

Figure 12 shows the phase error of the subsonic wavenumber for element length $h = 1.0$ cm and plate thickness $t = 0.5$ cm, giving the ratio $h/t = 2$. With this courser mesh, the error increases, yet the relative accuracy for the different methods remains the same, i.e. below the coincident frequency, the HLS-GLS combination shows the least error compared to HLS-STB and GGLS-GLS. Similar results are found for the leaky and evanescent roots (not shown).

Finally, we consider the dispersion relations obtained with a simplified variational equation where the fluid and coupling matrices $\mathbf{h}_{\mathrm{LS}}$ and $\mathbf{c}_{\mathrm{LS}}$ associated with the pressure loading in the structural residual R_1 are neglected in the formulation. In this case, the fluid and coupling matrices reduce to $h^e = h_{\mathrm{f}}$, and $q^e = c$, respectively, and symmetry is maintained. The subsonic

Copyright © 2001 John Wiley & Sons, Ltd.

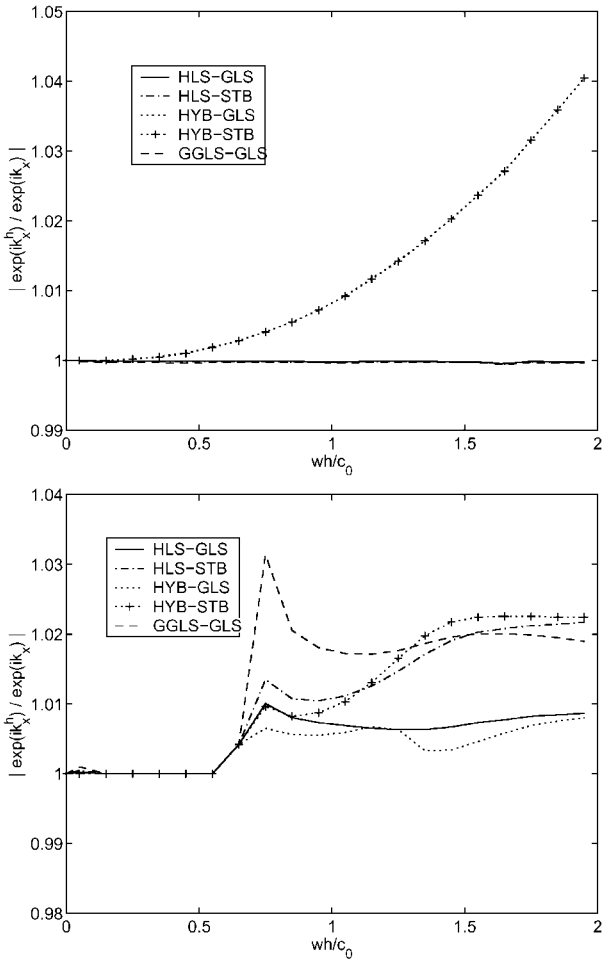

Figure 9. Relative error in imaginary part of wavenumber k_x for stabilized methods. (top) evanescent, (bottom) leaky.

wavenumber k_x for the HLS plate with GLS fluid, computed with, and without, the consistent coupling matrices $\mathbf{h}_{\mathrm{LS}}$ and $\mathbf{c}_{\mathrm{LS}}$ is shown in Figure 13 for fixed element length $h = 1.0$, and variable plate thickness t. As the normalized frequency increases, the finite element roots are limited by the value $k_x h = \pi$, corresponding to the minimum resolution of two elements per wavelength. An interesting observation is that for the higher element length-to-thickness h/t ratios, after the limit of $k_x h = \pi$ has been reached, the numerical wavenumber decreases before approaching the slope of the sonic wavenumber $k_0 h = \omega h / c_0$. In this course mesh region, the formulation which neglects the coupling matrices $\mathbf{h}_{\mathrm{LS}}$ and $\mathbf{c}_{\mathrm{LS}}$ displays less error than the consistent formulation; albeit both errors are large. In the region before reaching the limit of resolution, the consistent formulation displays slightly less error than the formulation which

Copyright © 2001 John Wiley & Sons, Ltd.

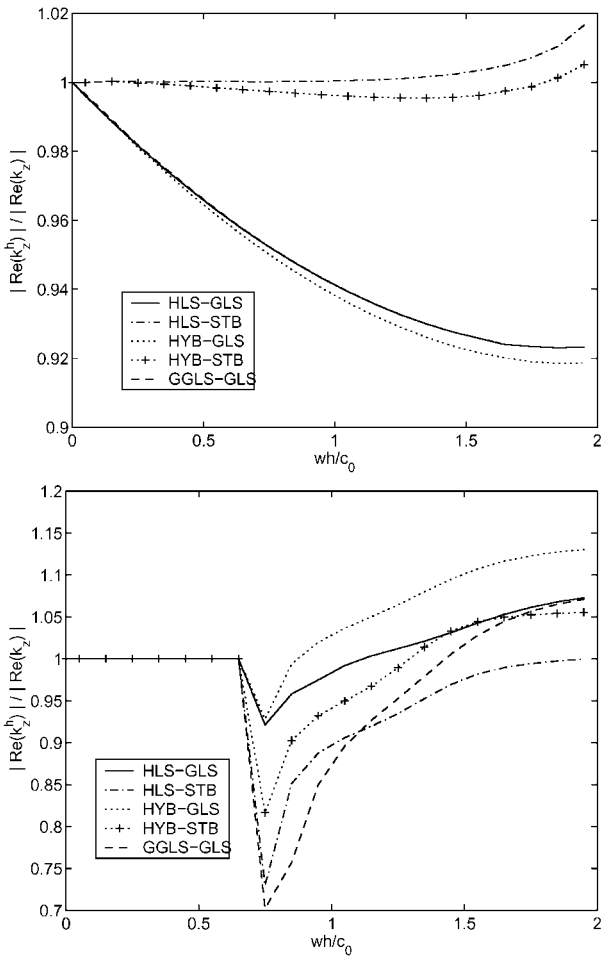

Figure 10. Relative error in real part of wavenumber k_z for stabilized methods. (top) evanescent, (bottom) leaky.

neglects the mesh parameter r_1 in the coupling and fluid matrices. This later observation is quantified in Figure 14 where the relative error in the numerical subsonic wavenumber compared to the analytic wavenumber is plotted. The results show a small improvement in accuracy when the coupling matrices $\mathbf{h}_{\mathrm{LS}}$ and $\mathbf{c}_{\mathrm{LS}}$ are included in the consistent formulation. For finer meshes, the results show that the matrices can be neglected with very small loss in accuracy. This same observation is observed in Figure 15 where the relative error in the subsonic wavenumber is compared for a constant plate thickness $t = 1.0$ cm, and element length ranging from $h = 1.0$ to 3.0 cm. Again for the steel plate interacting with water, the results with the coupling matrices $\mathbf{h}_{\mathrm{LS}}$ and $\mathbf{c}_{\mathrm{LS}}$ included exhibit a low-order perturbation to the subsonic root. Similar observations are found for the leaky and evanescent roots (not shown).

Copyright © 2001 John Wiley & Sons, Ltd.

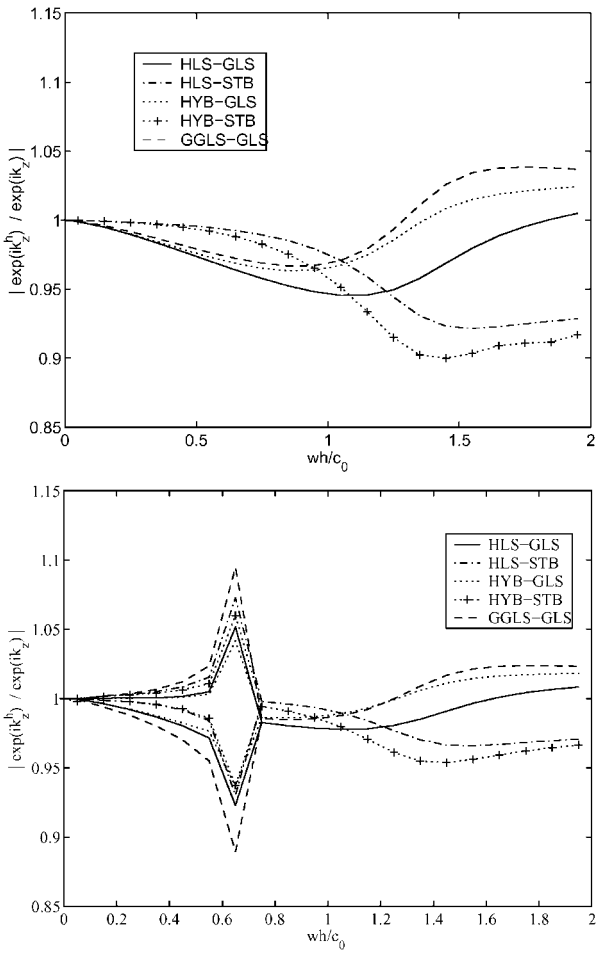

Figure 11. Relative error in imaginary part of wavenumber k_z for stabilized methods. (top) subsonic, (bottom) leaky.

6. CONCLUSIONS

A complex-wavenumber dispersion analysis of acoustic fluid interaction with Reissner–Mindlin plates is performed to quantify the accuracy of new stabilized finite element methods. Dispersion analysis provides a tool for comparing the free waves in different finite element formulations for fluid-loaded plates. The analysis of free waves in an infinite mesh allows us to predict the trends in behaviour of the elements when used to model boundary value problems with fixed boundaries. Results demonstrate the significantly improved accuracy of the hybrid least-squares (HLS) plate element developed in References [2, 3], combined with a GLS [4] or stabilized STB [5], fluid treatment, compared to the underlying hybrid (HYB)

Copyright © 2001 John Wiley & Sons, Ltd.

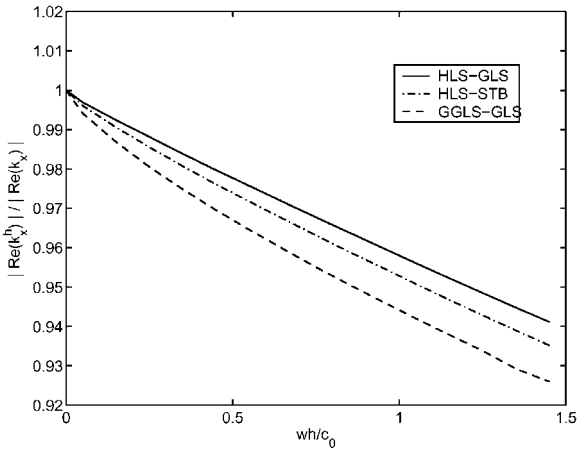

Figure 12. Relative error in the subsonic wavenumber k_x for stabilized methods with element length $h = 1.0$, and plate thickness $t = 0.5$.

element [15], and the displacement-based elements (MITC4) [1], and (GGLS) [14]. MITC4 plate elements coupled with a Galerkin fluid approximation performs poorly for both subsonic, evanescent, and leaky wavenumber components. The accuracy of the assumed-stress hybrid element (HYB), coupled with a GLS fluid treatment, is improved compared to MITC and performs well. Using the least-squares modification for the hybrid plate (HLS), together with GLS fluid elements, the performance of the hybrid element is enchanced further, especially in the difficult high-frequency region, yielding a highly accurate fluid-loaded plate model. The least-squares modifications are simple to implement with negligible increase in computational cost and memory. We note that instead of using stabilized low-order methods as studies here, high-order accuracy may also be achieved by 'brute-force' using higher-order finite element approximations such as hp-version or spectral extensions [19]. The inclusion of residuals on inter-element boundaries in the acoustic fluid as described in (STB) Reference [5], further improves the accuracy of the sonic wavenumber approximation. As a result, the accuracy is improved in the frequency regions where the acoustic discretization dominates the behaviour of the fluid-loaded plate. In particular, the accuracy is improved for (1) the subsonic wavenumber beyond the coincidence frequency, and (2) radiation in the perpendicular direction to the plate, due to evanescent waves along the plate.

In general, the ability to represent all wavenumber components is important. However, for common plate structures with relatively wide spacing between discontinuities, the subsonic wavenumber often plays a dominant role, and should be accurately represented in the finite element approximation. The HLS approach has a lower error than the GGLS approach for the important subsonic wavenumber. While GLS is not as accurate in approximating the sonic wavenumber compared to STB, in the range of frequencies prior to coincidence, the fluid phase error tends to partially cancel the plate discretization error leading to the best overall dispersion accuracy using the HLS-GLS structure–fluid combination.

In this paper, accurate methods for fluid-loaded plates were obtained using a consistent and symmetric variational formulation in combination with mesh parameters optimized for

Copyright © 2001 John Wiley & Sons, Ltd.

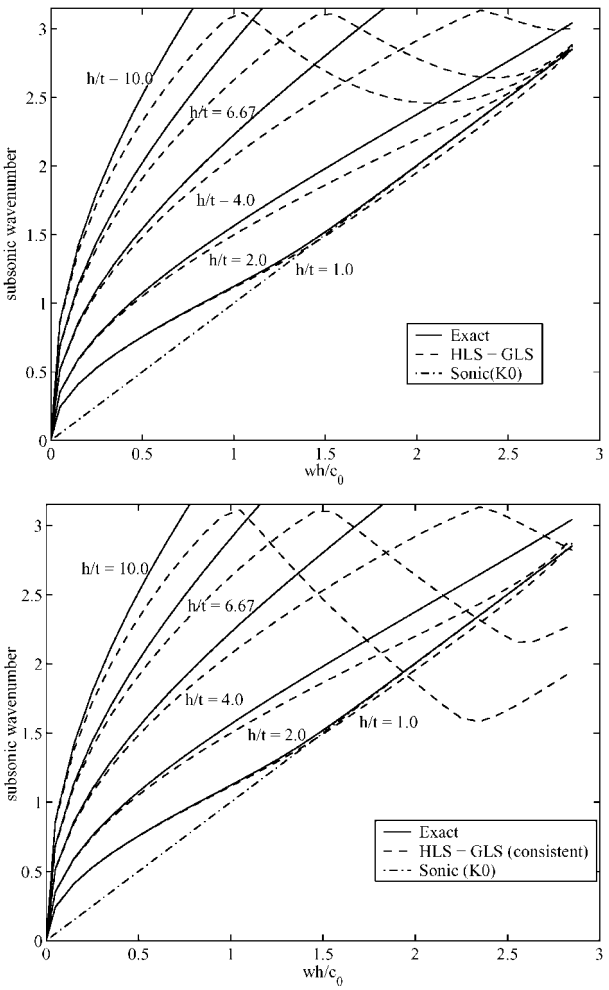

Figure 13. Subsonic wavenumber k_x versus normalized frequency for element length $h = 1.0$ and plate thickness $t = 1.0, 0.5, 0.25, 0.15, 0.1$. (top) Neglecting mesh parameter r_1 in coupling and fluid matrices. (bottom) Consistent coupling.

the uncoupled problems. We found that the fluid and coupling matrices resulting from the pressure loading appearing in the residual included in the least-squares modification to the plate equations results in a small improvement in accuracy in the numerical wavenumber–frequency relations for fluid-loaded plates. We conjecture that further improvements can be made by determining optimal design parameters within the HLS-GLS framework which are specifically tailored to match the dominant roots of the coupled fluid–structure dispersion relations.

Copyright © 2001 John Wiley & Sons, Ltd.

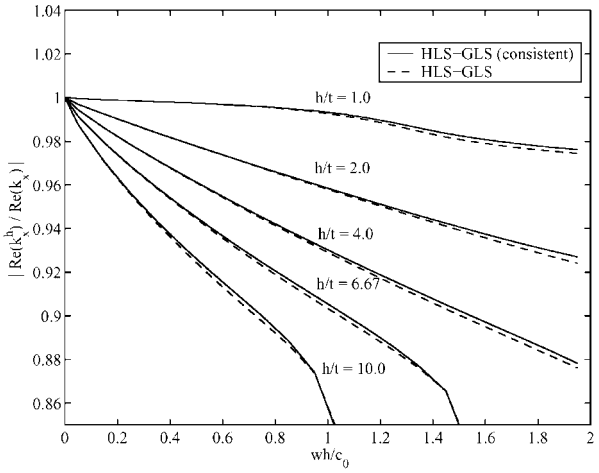

Figure 14. Relative error in real part of subsonic wavenumber k_x for element length $h = 1.0$ and plate thickness $t = 1.0, 0.5, 0.25, 0.15, 0.1$, with and without consistent coupling.

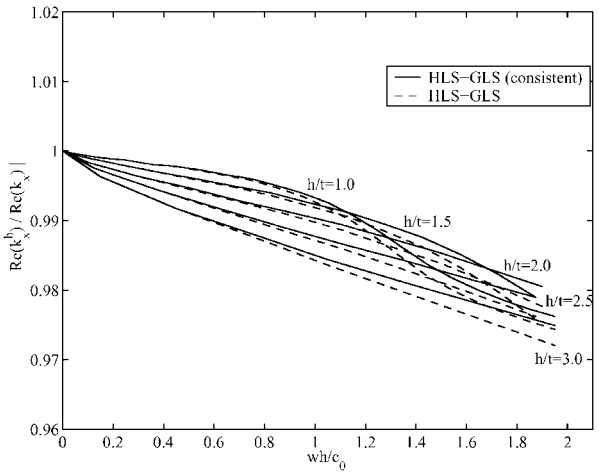

Figure 15. Relative error in real part of subsonic wavenumber k_x for plate thickness $t = 1.0$, and element length $h = 1.0, 1.5, 2.0, 3.0$, with and without consistent coupling.

ACKNOWLEDGEMENTS

Support for this work was provided by the National Science Foundation under Grant CMS-9702082 in conjunction with a Presidential Early Career Award for Scientists and Engineers (PECASE), and is gratefully acknowledged.

Copyright © 2001 John Wiley & Sons, Ltd.

REFERENCES

1. Bathe KJ, Dvorkin E. A four node plate bending element based on Mindlin–Reissner plate theory and mixed interpolation. *International Journal for Numerical Methods in Engineering* 1985; **21**:367–383.
2. Thompson LL, Tong Y. Hybrid least squares finite element methods for Reissner–Mindlin plates. *Proceedings of the ASME Noise Control and Acoustics Division—1999*, 1999 ASME International Mechanical Engineering Congress and Exposition, ASME, 1999; NCA-Vol. 26:77–89.
3. Thompson LL, Tong Y. Hybrid least squares finite element methods for Reissner–Mindlin plates. *Computer Methods in Applied Mechanics and Engineering*, accepted with revisions.
4. Thompson LL, Pinsky PM. A Galerkin least squares finite element method for the two-dimensional Helmholtz equation. *International Journal for Numerical Methods in Engineering* 1995; **38**:371–397.
5. Oberai AA, Pinsky PM. A residual-based finite element method for the Helmholtz equation. *International Journal for Numerical Methods in Engineering* 2000; **49**:399–419.
6. Jasti R. Mixed shell finite elements with applications in structural acoustics, Chapter 8. Ph.D. Dissertation, Stanford University, 1992.
7. Grosh K, Pinsky PM. Complex wave-number dispersion analysis of Galerkin and Galerkin least-squares methods for fluid-loaded plates. *Computer Methods in Applied Mechanics and Engineering* 1994; **113**:67–98.
8. Hughes TJR, Franca LP, Hulbert GM. A new finite element formulation for computational fluid dynamics: VIII. The Galerkin least squares method for advective-diffusive equations. *Computer Methods in Applied Mechanics and Engineering* 1989; **73**:173–189.
9. Harari I, Hughes TJR. Galerkin/least-squares finite element methods for the reduced wave equation with non-reflecting boundary conditions in unbounded domains. *Computer Methods in Applied Mechanics and Engineering* 1992; **98**:411–454.
10. Harari I, Grosh K, Hughes TJR, Malhotra M, Pinsky PM, Stewart JR, Thompson LL. Recent developments in finite element methods for structural acoustics. *Archives of Computational Methods in Engineering* 1996; **3**:132–311.
11. Hughes TJR, Franca LP. A mixed finite element method formulation for Reissner–Mindlin plate theory: uniform convergence of all higher-order spaces. *Computer Methods in Applied Mechanics and Engineering* 1988; **67**: 223–240.
12. Grosh K, Pinsky PM. Galerkin generalized least-squares methods for timoshenko beams. *Computer Methods in Applied Mechanics and Engineering* 1996; **132**:1–16.
13. Franca LP, Dutra do Carmo DG. The Galerkin gradient least-squares method. *Computer Methods in Applied Mechanics and Engineering* 1979; **74**:44–54.
14. Grosh K, Pinsky PM. Galerkin generalized least squares methods for time-harmonic structural acoustics. *Computer Methods in Applied Mechanics and Engineering* 1998; **154**:299–318.
15. Aminpour MA. An assumed-stress Hybrid 4-node shell element with drilling degrees of freedom. *International Journal for Numerical Methods in Engineering* 1992; **33**:19–38.
16. Crighton DG. The free and forced waves on fluid-loaded elastic plate. *Journal of Sound and Vibration* 1979; **63**(2):225–235.
17. Crighton DG. The 1988 Rayleigh medal lecture: fluid loading—the interaction between sound and vibration. *Journal of Sound and Vibration* 1988; **133**:1–27.
18. Grosh K. Residual-based methods for fluid-loaded beams. *Computer Methods in Applied Mechanics and Engineering*, to appear.
19. Thompson LL, Pinsky PM. Complex wavenumber Fourier analysis of the p-version finite element method. *Computational Mechanics* 1994; **13**(4):255–275.
20. Sankar S. Complex wavenumber dispersion analysis of residual based finite element methods for acoustic fluid–structure interaction. *M.S. Thesis*. Clemson University, Department of Mechanical Engineering, August 2000.
21. Mullen R, Belytschko T. Dispersion analysis of finite element semidiscretizations of the two-dimensional wave equation. *International Journal for Numerical Methods in Engineering* 1982; **18**:11–29.

Copyright © 2001 John Wiley & Sons, Ltd.